Why three? A cone-geometry derivation of the integrable swinging Atwood's machine

N Tufillaro

Aqualytics, PO Box 1028, Corvallis, Oregon 97333, USA

nick@aqualytics.eco

Abstract

The swinging Atwood's machine can be used in classical mechanics courses to study chaotic and integrable dynamics. The standard demonstration of integrability proceeds by a canonical transformation at $\mu = M/m = 3$; however, it arrives without motivation. This paper replaces the guess with a derivation. Writing the kinetic energy as a Riemannian metric on configuration space — the mass matrix *is* a metric — identifies the pulley as a cone point of total angle $2\pi/\sqrt{\mu+1}$. At $\mu = 3$ the angle is π, the cone admits a smooth double branched cover, and on the cover the Hamilton–Jacobi equation separates in parabolic coordinates. The treatment is self-contained, assumes no prior differential geometry, and is intended for advanced undergraduate and beginning graduate courses; nine problems, sorted by classroom setting, are supplied.

Keywords: swinging Atwood's machine, integrability, cone geometry, Hamilton–Jacobi separation, Riemannian metric, classical mechanics teaching

Submitted to: European Journal of Physics

1 Introduction

The swinging Atwood's machine (SAM) is built by connecting two masses as shown in figure 1: mass M moves only vertically while mass m can swing freely in a plane. Setting $m = 1$, defining $\mu = M/m$, and using polar (r, θ) coordinates, the Hamiltonian for SAM is [1, 2]

$$H = \frac{1}{2}\left(\frac{p_r^2}{\mu+1} + \frac{p_\theta^2}{r^2}\right) + gr(\mu - \cos\theta). \tag{1}$$

Its most striking property is that the motion is integrable [3] at the single mass ratio $\mu = 3$, and non-integrable at every other mass ratio with $\mu > 1$ [4, 5, 6].

1.1 Where the machine sits in the curriculum, and what is missing

SAM is treated as a worked problem in Lemos's *Analytical Mechanics* [1], it can be assembled from pulleys and string for the price of a laboratory afternoon, and it is accessible both theoretically and experimentally to undergraduates [7, 2, 8, 9, 5, 10].

The standard demonstration of the integrability at $\mu = 3$ starts with the ansatz of a canonical transformation

$$\xi = \sqrt{r\left(1+\sin\tfrac{\theta}{2}\right)}, \qquad \eta = \pm\sqrt{r\left(1-\sin\tfrac{\theta}{2}\right)}, \tag{2}$$

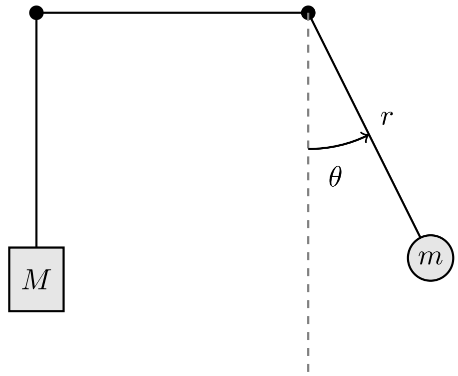

Figure 1: The swinging Atwood's machine. The mass M moves vertically on one side; the mass m swings in a plane on the other side, joined to M by an inextensible massless string over frictionless pulleys. The coordinates (r, θ) are polar coordinates of the swinging mass about its pulley, with θ measured from the downward vertical (dashed line).

and goes on to observe that at $\mu = 3$ the Hamilton–Jacobi equation separates [3, 9]. However, the derivation does not say where equation (2) comes from, why half-angles appear, why η carries a $\pm$, or what distinguishes the value three.

This paper shows how some elementary differential geometry can provide an answer. The solution is short enough to fit in one lecture and requires no differential geometry from outside this paper; section 11 describes how the material is organized for use in a course. The technique — view the mass matrix as a metric, and then examine the geometry as a function of the parameters — transfers to other systems (section 10) and has a deep history in classical mechanics [11].

1.2 Setting and symmetry

The potential $U = gr(\mu - \cos\theta)$ is positive when $\mu > 1$, and the accessible region of configuration space is called the Hill region

$$r \leq \frac{E}{g(\mu - \cos\theta)}. \tag{3}$$

For $\mu > 1$ the denominator is bounded away from zero, so the Hill region is a bounded topological disc containing the pulley, and every orbit at fixed energy is bounded. For $\mu \leq 1$ the boundary opens and unbounded orbits exist [12]. Throughout this paper $\mu > 1$ and the motion is confined to the disc (3). The swinging mass is set to $m = 1$, and numerical examples use SI units with $g = 9.81$ m s^{-2} and energy $E = 2g$. With these values the Hill region (3) at $\mu = 3$ has maximum radius $E/[g(\mu - 1)] = 1$ m, so "close to the pulley" means $r \ll 1$.

The Hamiltonian also carries a discrete symmetry. Because U depends on θ only through $\cos\theta$, equation (1) is invariant under the reflection $\mathcal{S} : (r, \theta, p_r, p_\theta) \mapsto (r, -\theta, p_r, -p_\theta)$, and also under time reversal $\mathcal{T} : (p_r, p_\theta) \mapsto (-p_r, -p_\theta)$, $t \mapsto -t$. Their composition $\mathcal{R} = \mathcal{S} \circ \mathcal{T}$, acting as $(r, \theta, p_r, p_\theta) \mapsto (r, -\theta, -p_r, p_\theta)$ with $t \mapsto -t$, is an anti-canonical involution, so SAM is a *reversible* system in the sense of Devaney [13]. Its fixed set has two components, $\theta = 0$ and $\theta = \pi$, each with $p_r = 0$; an orbit meeting the $\theta = 0$ component $\{\theta = 0,\ p_r = 0\}$ at two distinct times closes up, which is the standard route to SAM's symmetric periodic orbits [9, 8]. This $\mathbb{Z}_2$ structure is a first indication that the natural configuration space for SAM is not simply the (r, θ) half-plane; it reappears in a sharper form in section 5.

2 Mechanics as geometry

For a system whose kinetic energy is a homogeneous quadratic form in the velocities,

$$T = \tfrac{1}{2}\, g_{ab}(q)\, \dot{q}^a \dot{q}^b, \tag{4}$$

the coefficients g_{ab} are the components of a Riemannian metric on configuration space,

$$\mathrm{d}s^2 = g_{ab}(q)\, \mathrm{d}q^a \mathrm{d}q^b. \tag{5}$$

At each configuration it supplies an inner product on velocities, and the kinetic energy is half the squared length of the velocity vector.

By Maupertuis' principle the trajectories at fixed energy are geodesics of the conformally rescaled Jacobi metric $\tilde{g}_{ab} = 2[E - U]g_{ab}$ [14, 15, 16, 17], and cone geometry arises naturally from that metric: Montgomery constructs a cone of total angle $2\pi(1 - \beta/2)$ whose geodesics are the zero-energy orbits of $U \propto -r^{-\beta}$, from whose angle Rutherford-type scattering angles can be read directly [18]. The same construction appears in the Kepler and n-body settings [19, 20, 21].

Here we need only the weaker statement that the *kinetic* metric (5) is the geometry a free particle would feel when the potential is negligible. For orbits very close to the pulley ($r \ll 1$) the potential is indeed small, since it is proportional to r. For SAM the kinetic energy is

$$T = \tfrac{1}{2}(M + m)\dot{r}^2 + \tfrac{1}{2}mr^2\dot{\theta}^2 = \tfrac{1}{2}\left[(\mu + 1)\dot{r}^2 + r^2\dot{\theta}^2\right]. \tag{6}$$

The mass ratio μ acts asymmetrically on the radial and angular terms. Hence

$$\mathrm{d}s^2 = (\mu + 1)\, \mathrm{d}r^2 + r^2 \mathrm{d}\theta^2 \tag{7}$$

can be viewed as an *anisotropic* central metric. Its best-known cousin is Gutzwiller's anisotropic Kepler problem [22, 23], where the anisotropy is Cartesian — a direction-dependent effective mass — and produces chaos; in SAM the anisotropy is radial versus tangential, and the motion is chaotic at generic mass ratios yet integrable at $\mu = 3$.

3 The kinetic metric is a cone

Equation (7) is almost the metric of a free particle on a flat plane: it differs from the flat-plane metric only by the constant factor $\mu + 1$ in the radial term. Rescale

$$\rho = \sqrt{\mu + 1}\, r, \qquad \varphi = \frac{\theta}{\sqrt{\mu + 1}}. \tag{8}$$

Then $\mathrm{d}\rho^2 = (\mu + 1)\mathrm{d}r^2$ and $\rho^2 \mathrm{d}\varphi^2 = r^2 \mathrm{d}\theta^2$, so

$$\mathrm{d}s^2 = \mathrm{d}\rho^2 + \rho^2 \mathrm{d}\varphi^2 \tag{9}$$

is now the line element associated with a free particle in polar coordinates. The curvature vanishes everywhere except possibly at the origin.

Unlike θ, the physical angle of the swinging mass, the positional angle φ of a particle in this rescaled space does not run over the full range of 2π. Since θ is a physical angle of period 2π, equation (8) gives

$$\varphi \sim \varphi + \alpha, \qquad \alpha(\mu) = \frac{2\pi}{\sqrt{\mu + 1}}. \tag{10}$$

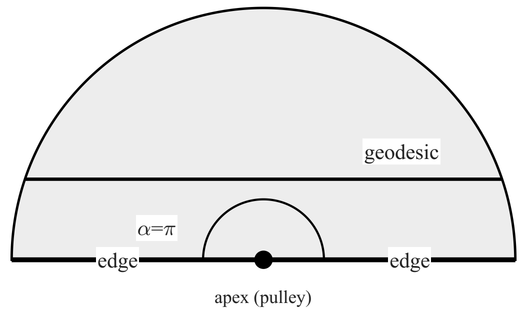

Figure 2: The unrolled cone at $\mu = 3$. A wedge of angle $2\pi - \alpha$ has been removed from the plane and the two radii marked "edge" identified; the apex is the pulley, and the arc at the apex marks the total angle $\alpha = \pi$. A close passage of the swinging mass to the pulley is nearly free motion, hence a straight line in this developed picture, whose swept angle approaches $\Delta\varphi = \pi$ between large radii.

A flat metric whose angular coordinate closes after less than 2π is a *cone*, and α is its total angle (figure 2). SAM has been viewed as motion on a cone before [24]; what follows works with the intrinsic cone of the kinetic metric and, crucially, with its total angle.

It is helpful at this point to make a cone with paper, scissors and a bit of tape — in a lecture this takes two minutes and is worth the interruption. Cut a paper disc along a radius, remove a wedge, tape the edges: the result is intrinsically flat except at the apex, where the curvature concentrates as a delta function of strength $2\pi - \alpha$, the angle deficit, as the Gauss–Bonnet theorem requires [25]. The pulley is a cone point of the configuration-space geometry, and the mass ratio alone sets its angle.

Two remarks place this geometry in context. Cones of angle $2\pi/n$ with n integer are the quotients $\mathbb{C}/\mathbb{Z}_n$, the *orbifold* points of two-dimensional geometry [25, 26]. A cone point is also where regularization theory operates: Levi-Civita's map $z \mapsto z^2$ removing the Kepler collision [27, 28, 29] is precisely the double branched cover of a cone of angle π. We use it, in reverse, in section 5.

4 A physical consequence, and a check

The cone angle has a testable consequence. Near the pulley the potential tends to zero while the kinetic energy stays finite, so a fast close passage is nearly free motion — a straight line in the developed cone. A straight line passing close to the apex sweeps a total angle approaching π between large radii, so $\Delta\varphi \to \pi$, and by equation (8)

$$\Delta\theta = \pi\sqrt{\mu + 1}, \qquad W(\mu) = \frac{\sqrt{\mu+1}}{2} \text{ turns,} \tag{11}$$

the limiting value as the angular momentum $p_\theta \to 0$, equivalently as the closest approach goes to zero; for true collision orbits the relation is exact. The rotation of a close passage about the pulley is thus $W(\mu)$ turns, the quantity plotted in figure 3.

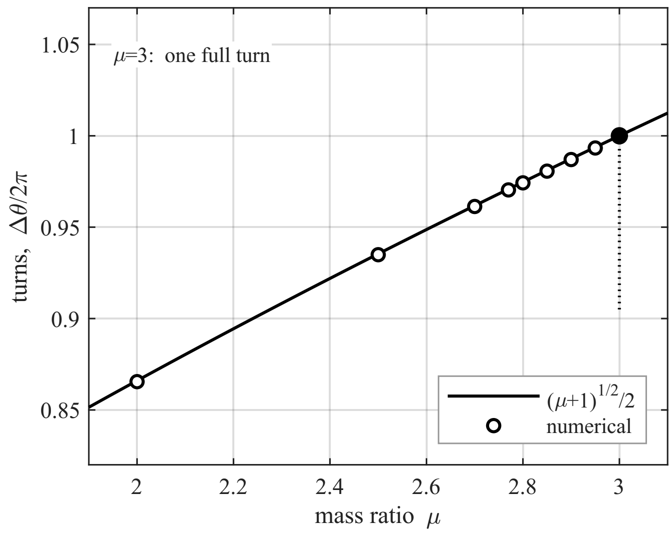

Figure 3: The deflection law (11) against direct numerical integration of the regularized equations of motion at $p_\theta = 10^{-5}$, $E = 2g$. Agreement is at the 10^{-3} level and improves as $p_\theta \to 0$. At $\mu = 3$ the passage is exactly one full turn.

Equation (11) was first derived in [30], by direct analysis of the collision orbits, in the form $\theta_e = \pm\pi\sqrt{\mu+1}+\theta_i$. The argument here is the same one used in [18] to obtain Rutherford scattering angles from a conical Jacobi–Maupertuis metric. Figure 3 compares equation (11) with numerical integration of the regularized equations [10].

Equation (11) might be initially surprising because it contains no parameters other than μ. At $\mu = 3$, equation (11) gives exactly one full turn: a mass falling nearly onto the pulley wraps once and leaves along the direction it arrived from. This is the tightly wrapped "unstable loop" orbit [10], and its closure is a first sign that $\mu = 3$ is geometrically distinguished.

5 $\mu = 3$: the angle is π, the cover is smooth

Set $\mu = 3$ in equation (10): $\alpha(3) = 2\pi/\sqrt{4} = \pi$. The cone is $\mathbb{C}/\mathbb{Z}_2$, the plane modulo the half-turn $z \mapsto -z$.

This is the crucial fact, because a cone of angle π has a *smooth* double cover. Going once around the apex advances φ by π; going twice advances it by 2π and closes. The two-fold cover therefore has total angle 2π: an ordinary complete Euclidean plane with no singular point at all. (The smoothness is that of the metric; the lifted potential, equation (15) below, remains continuous but not differentiable at $q = 0$.) The deck transformation exchanging sheets is $\theta \mapsto \theta + 2\pi$, that is, $q \mapsto -q$ in the Cartesian coordinates of equation (12) below.

Since $\varphi = \theta/2$ here, the cover is described by letting θ run over $[0, 4\pi)$, so the *half-angle* $\theta/2$ becomes a genuine single-valued angle. That is the origin of the half-angles in equation (2), and of its $\pm$: the sign labels the sheet. Define

$$q_1 = 2r\sin\tfrac{\theta}{2}, \qquad q_2 = 2r\cos\tfrac{\theta}{2}, \qquad |q| = 2r. \tag{12}$$

The reflection symmetry of section 1.2 takes a sharper form on the cover. The reflection $\mathcal{S}$ acts on the coordinates (12) as $q_1 \mapsto -q_1$, while the deck transformation $q \mapsto -q$ is the composition

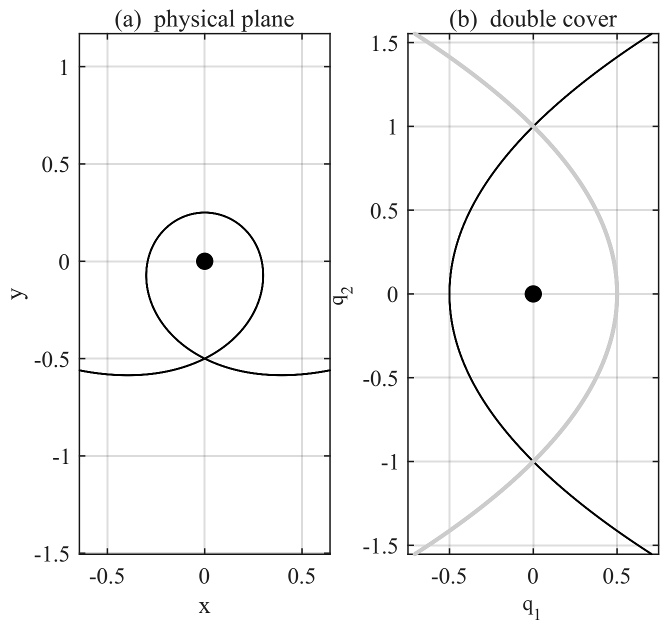

Figure 4: A trajectory at $\mu = 3$, $E = 2g$. (a) In physical configuration space, where the pulley is a cone point; the Cartesian coordinates are $x = r\sin\theta$, $y = -r\cos\theta$. (b) Lifted to the smooth double cover via equation (12), shown together with its image under the deck transformation $q \mapsto -q$ (grey). The two curves are the two lifts of the same physical orbit, one on each sheet.

of the two coordinate reflections $q_1 \mapsto -q_1$ and $q_2 \mapsto -q_2$. In this sense the physical reflection symmetry is one factor of the covering involution. Both $\mathcal{S}$ and the deck map send the second integral I constructed in section 8 [equation (21)] to $-I$.

6 On the cover, the kinetic energy is free

Differentiating equation (12) and using $\rho = 2r$, $\varphi = \theta/2$,

$$\tfrac{1}{2}|\dot{q}|^2 = \tfrac{1}{2}(\dot{\rho}^2 + \rho^2\dot{\varphi}^2) = \tfrac{1}{2}\left(4\dot{r}^2 + r^2\dot{\theta}^2\right) = T, \tag{13}$$

that is, $T = \frac{1}{2}|\dot{q}|^2$: the kinetic energy of a *free particle of unit mass in a plane* (figure 4).

The anisotropy has vanished. The factor $\mu + 1 = 4$ distinguishing radial from tangential inertia — the very thing that makes SAM harder than a pendulum — has been absorbed exactly by the change of coordinates. All of the remaining difficulty now sits in the potential.

7 The potential, and recognizing separability

Rewrite $U = gr(3 - \cos\theta)$ on the cover. With $\cos\theta = 1 - 2\sin^2(\theta/2)$ and $r = |q|/2$,

$$U = g|q|\left(1 + \sin^2\tfrac{\theta}{2}\right), \tag{14}$$

and since $\sin(\theta/2) = q_1/|q|$,

$$U = g\left(|q| + \frac{q_1^2}{|q|}\right). \tag{15}$$

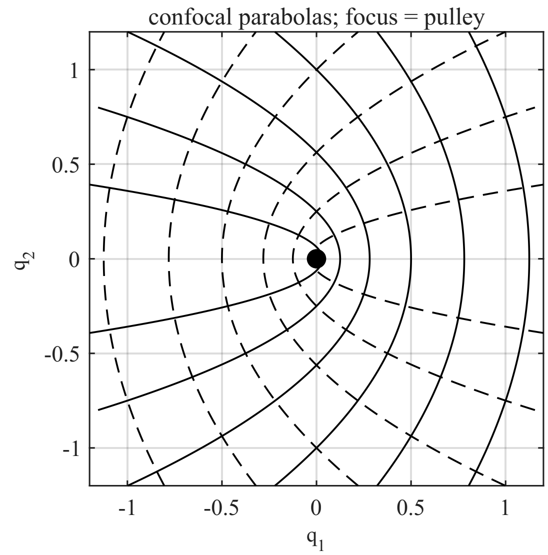

Figure 5: Parabolic coordinates (16) on the double cover. Solid curves are constant ξ, dashed constant η. All are confocal parabolas whose common focus is the pulley.

This is the recognition step, the one place where a working familiarity with a variety of coordinate transformations is needed to push the solution forward. Introduce the parabolic coordinates (ξ, η) on the cover by

$$q_1 = \tfrac{1}{2}(\xi^2 - \eta^2), \qquad q_2 = \xi\eta, \tag{16}$$

so that $|q| = \frac{1}{2}(\xi^2 + \eta^2)$ and $\mathrm{d}q_1^2 + \mathrm{d}q_2^2 = (\xi^2 + \eta^2)(\mathrm{d}\xi^2 + \mathrm{d}\eta^2)$.

The use of parabolic coordinates is motivated by looking at the Hamiltonian with free kinetic energy and noting that it separates in these coordinates precisely when $(\xi^2 + \eta^2)U$ is of Liouville form, a sum $f(\xi) + h(\eta)$ with no cross term. For a general potential of the present shape, $U = a|q| + b\, q_1^2/|q|$,

$$(\xi^2 + \eta^2)\, U = \frac{a+b}{2}\left(\xi^4 + \eta^4\right) + (a-b)\, \xi^2\eta^2, \tag{17}$$

so neither term separates on its own — each contributes a cross term $\pm\, \xi^2\eta^2$ — and the sum is of Liouville form if and only if $a = b$, the two cross terms canceling.

Equation (15) has $a = b = g$, and that is why it separates. The canonical physical example of parabolic separability is the Stark effect, $U = -k/|q| - Fq_1$, which separates in parabolic coordinates [31, 14, 32]; there, however, each term separates individually, while here separation is a cancellation between two terms neither of which separates alone. The contrast is a good exercise in what "separable" actually asserts. The same cancellation returns in section 9, where it fixes the potential role of the mass ratio.

8 Separation, and the second integral

The parabolic coordinates (16) introduced in section 7 have level curves that are confocal parabolas with focus at the pulley (figure 5). Comparing with equation (12) gives $\xi^2 = 2r(1 + \sin\frac{\theta}{2})$ and $\eta^2 = 2r(1 - \sin\frac{\theta}{2})$: equation (2), recovered up to an overall factor $\sqrt{2}$, a canonical rescaling absorbed into the unit-mass normalization on the cover, with the $\pm$ now identified as the choice of sheet.

The potential becomes $U = g(\xi^4+\eta^4)/(\xi^2+\eta^2)$, and with $p_\xi = (\xi^2+\eta^2)\dot\xi$, $p_\eta = (\xi^2+\eta^2)\dot\eta$,

$$H = \frac{p_\xi^2 + p_\eta^2}{2(\xi^2+\eta^2)} + \frac{g(\xi^4+\eta^4)}{\xi^2+\eta^2}. \tag{18}$$

This is of *Liouville form* [33, 34], and such Hamiltonians always separate. Setting $H = E$ and multiplying by $\xi^2+\eta^2$,

$$\underbrace{\left[\tfrac{1}{2}p_\xi^2 + g\xi^4 - E\xi^2\right]}_{K} + \underbrace{\left[\tfrac{1}{2}p_\eta^2 + g\eta^4 - E\eta^2\right]}_{-K} = 0. \tag{19}$$

The first bracket depends only on (ξ, p_ξ), the second only on (η, p_η), yet they sum to zero; each is therefore constant. Eliminating E between them gives an integral independent of the energy shell,

$$K = \frac{\eta^2 p_\xi^2 - \xi^2 p_\eta^2}{2(\xi^2+\eta^2)} + \frac{g\,\xi^2\eta^2(\xi^2-\eta^2)}{\xi^2+\eta^2}. \tag{20}$$

Rewriting equation (20) in the physical variables $(r, \theta, p_r, p_\theta)$ is a short but fiddly calculation, set out in the appendix. The result is

$$I = p_r p_\theta \cos\tfrac{\theta}{2} - \frac{2p_\theta^2}{r}\sin\tfrac{\theta}{2} + 4gr^2\cos^2\tfrac{\theta}{2}\sin\tfrac{\theta}{2}. \tag{21}$$

This is, up to normalization, the integral exhibited by Hamilton–Jacobi methods in [3] and restated as Theorem 7.6 of [5]; the constant is the total mass $\mu + 1 = 4$ absorbed by the unit-mass normalization on the cover.

The Poisson bracket of I with the Hamiltonian at general mass ratio carries a single explicit factor of $\mu - 3$:

$$\begin{aligned}\{H_\mu, I\} \quad = \quad & \frac{(\mu-3)}{2r^2(\mu+1)}\Big[p_r p_\theta^2 \sin\tfrac{\theta}{2} + 2g(1+\mu)p_\theta r^2\cos\tfrac{\theta}{2} \\ & \qquad +4gp_r r^3\cos^2\tfrac{\theta}{2}\sin\tfrac{\theta}{2}\Big].\end{aligned} \tag{22}$$

The bracket vanishes identically at $\mu = 3$ and at no other mass ratio, and $\mu = 3$ is a simple root: I fails to commute with H_μ at first order in $\mu - 3$, not at some degenerate higher order. Equation (22) is the result of a lengthy but routine computer-algebra computation, which Problem 6 invites the reader to reproduce.

8.1 A parity that explains an old puzzle

Under the deck transformation $\theta \mapsto \theta + 2\pi$ the half-angle functions $s = \sin(\theta/2)$ and $c = \cos(\theta/2)$ obey $s \mapsto -s$ and $c \mapsto -c$, so *every* term of equation (21) changes sign:

$$H \mapsto H, \qquad I \mapsto -I. \tag{23}$$

The Hamiltonian descends to physical configuration space; the integral does not. Only I^2 is single-valued downstairs.

SAM's "hidden" constant is therefore hidden because it does not live downstairs. It is a function on the double cover, and the cover is exposed by looking at the cone angle π. For a student this is a concrete answer to a question that is usually left rhetorical — why some conserved quantities are easy to spot and others are not.

9 Necessary, but not sufficient

The cone does not explain everything. The ratio μ plays two logically independent roles in equation (1): a *kinematic* role in the metric and a *potential* role in $gr(\mu - \cos\theta)$. Name them μ_{kin} and μ_{pot}.

The *double* cover is smooth if and only if $\sqrt{\mu_{\text{kin}}+1} = 2$, i.e. $\mu_{\text{kin}} = 3$. That is geometry. Expanding $(\xi^2+\eta^2)U$ with general μ_{pot} repeats the computation of equation (17), with the coefficients now carrying the mass ratio: on the cover $U = \frac{1}{2}g(\mu_{\text{pot}} - 1)|q| + g\,q_1^2/|q|$, so $a = \frac{1}{2}g(\mu_{\text{pot}} - 1)$ and $b = g$, and the condition $a = b$ reads $\mu_{\text{pot}} = 3$. The cross term $(a-b)\,\xi^2\eta^2$ becomes $\frac{1}{2}g(\mu_{\text{pot}}-3)\,\xi^2\eta^2$, which spoils the Liouville form and vanishes if and only if $\mu_{\text{pot}} = 3$. That is dynamics.

Two independent conditions, each demanding the value 3, are met simultaneously. The cone explains why a smooth cover exists and why the kinetic term trivializes; it does not by itself explain separability. SAM is integrable at $\mu = 3$ because of a coincidence between its geometry and its dynamics.

The same distinction settles a related puzzle. Finite-order cone points occur whenever $\sqrt{\mu+1}$ is an integer, $\mu = n^2 - 1 = 3, 8, 15, 24, 35, \ldots$, yet the collision is regularizable [30] only for $\mu = 3, 15, 35, \ldots$. The criterion is not orbifold-ness but whether the deflection πn of equation (11) is a multiple of 2π, requiring n even. Odd n gives an orbifold point that is nonetheless non-regularizable, incoming and outgoing rays differing by π.

Neither condition implies integrability. Ziglin-theoretic analysis [4, 35] shows that SAM is non-integrable for every mass ratio outside the countable family

$$\mu_p = 1 + \frac{4}{p^2+p-4}, \qquad p = 2, 3, 4, \ldots, \tag{24}$$

every member of which lies in $(1, 3]$: $\mu_2 = 3$, $\mu_3 = 3/2$, $\mu_4 = 5/4$, $\mu_5 = 15/13$, and $\mu_p \to 1$ as $p \to \infty$. For $p > 2$ the first-order variational equations are inconclusive, and Martínez and Simó closed these degenerate cases using higher-order variational equations and differential Galois theory [6, 36]; consequently $\mu = 3$ is the only integrable mass ratio with $\mu > 1$. The finite-order cone points $\mu = n^2 - 1 = 8, 15, 24, 35, \ldots$ with $n > 2$ lie outside the family (24) and are non-integrable already by the first-order argument.

Separability is possible, but should not be expected, in generalizations: in the three-dimensional machine, and in variants adding Coulomb or Hooke interactions (the latter only under further conditions on the couplings), integrable cases persist at $\mu = 3$, but non-integrable motion is usually the norm once rotational symmetry is broken [7, 37].

10 The method beyond the machine

The specific result — integrability at $\mu = 3$ — belongs to one machine. The method, though, transfers to other physical systems. Three steps can be identified:

1. *View the mass matrix as a metric.* Whenever the kinetic energy is a quadratic form in the velocities, equation (5) turns the inertia of the system into the geometry of its configuration space. No approximation is involved.

2. *Look for the singular points of that geometry.* They sit where coordinates degenerate, which is usually where the physics is hardest — collisions, coincidences, pivots. Compute the total angle around each.

3. *Ask when the angle is a submultiple of* 2π*.* If it is $2\pi/n$ the singular point is an orbifold point and there is a smooth n-fold branched cover on which the geometry is ordinary. Parameter values that make this happen are exactly the values at which the system may simplify.

Other cases where this method can be helpful are: Levi-Civita's regularization of the Kepler collision [27, 28, 29]; Montgomery's cone construction to recover the Rutherford scattering angles from a conical Jacobi–Maupertuis metric [18]; the geometric phase acquired on a circuit around a conical intersection in molecular physics [38, 39]; and the sign change of a spin-$\frac{1}{2}$ wavefunction under a 2π rotation, which involves a more mysterious use of a double cover. The deeper lesson in these examples is to ask what the configuration space looks like before focusing on what individual trajectories do.

11 Using this in the classroom

Level and prerequisites. The material is aimed at advanced undergraduates and beginning graduate students, and fits most naturally in a second course in classical mechanics at the point where Hamilton–Jacobi theory and separation of variables are introduced. It requires Lagrangian and Hamiltonian mechanics, plane polar coordinates, and comfort with a change of variables. It requires no prior differential geometry: sections 2 and 3 develop everything that is used.

Sequencing. Sections 2 to 4 — metric, cone, cone angle, deflection law — form a self-contained first lecture, with the paper-and-scissors cone built in the room and the deflection law equation (11) as its payoff. A class that stops there has still learned a method and a testable prediction. Sections 5 to 8 — cover, free kinetic energy, separation, second integral — form a second lecture for a course that has already met Hamilton–Jacobi separation. Section 9 is short and can be given as reading; it is, however, the section most worth discussing, because it is a rare worked example in which a satisfying explanation is shown to be incomplete.

Problems. The problems are grouped by setting rather than difficulty. Problem 1 needs only paper, scissors and a ruler, and belongs in the lecture room; problems 2 and 3 are pencil-and-paper exercises at the level of the course; problems 4 and 5 are short plotting exercises suitable for a first homework in any language the students already use; problems 6 and 7 require a computer-algebra system and a numerical integrator respectively, and suit a computational-physics course; problem 8 is open-ended enough for a short student project, since the numerical conjecture it states is unresolved; and problem 9 is a discussion question with no single right answer.

12 Problems

Problem 1. Take a paper disc and draw a straight line across it, passing close to the center. Now remove a wedge of angle $2\pi - \alpha$ and tape the cut edges together to make a cone; choose $\mu \leq 3$, so that $\alpha \geq \pi$ and the line you drew fits inside the retained sector. Verify that the line has become a geodesic whose swept angle in the cone coordinate approaches π as its distance from the center goes to zero, and relate this to equation (11).

Problem 2. Show that a cone of angle $2\pi/n$ is the quotient of the plane by a rotation of order n, and that its smooth branched cover is n-fold. Why does $n = 2$ have the special property that the deck transformation is $q \mapsto -q$?

Problem 3. Using equation (16), sketch curves of constant ξ and η in the (q_1, q_2) plane. Confirm they are confocal parabolas with focus at the origin, and explain physically why the pulley should be the focus.

Problem 4. Plot the Hill-region boundary $r = E/[g(\mu - \cos\theta)]$ at $E = 2g$ for $\mu = 3$, 2.9 and 2.8. Verify that the region is a topological disc containing the pulley. Then repeat for $\mu = 1.5$, 1.2 and 1.05 and show that, although the region remains a bounded disc for every $\mu > 1$, its maximum radius $E/[g(\mu - 1)]$ grows without bound as $\mu \to 1$.

Problem 5. Plot the cone angle $\alpha(\mu) = 2\pi/\sqrt{\mu + 1}$ over $1 \leq \mu \leq 35$ and mark the values of μ for which $\sqrt{\mu + 1}$ is an integer. Which of these are regularizable, and why is the regularizability criterion not the same as the orbifold condition that $\sqrt{\mu + 1}$ be an integer?

Problem 6. Compute $\{H_\mu, I\}$ symbolically at general mass ratio and verify equation (22). Confirm that the bracket vanishes identically at $\mu = 3$ and at no other value of μ.

Problem 7. Integrate the equations of motion numerically at $\mu = 3$ and $\mu = 2.9$, starting from $r_0 = 0.50$, $\theta_0 = 0$, $p_{r0} = 6.26$, with $p_{\theta 0}$ then fixed by $E = 2g$ (at $\mu = 3$ this gives $p_{\theta 0} = 1.5671$), and plot I of equation (21) against time over sixty time units. Confirm that I is conserved at $\mu = 3$ (to about 10^{-11} with a high-order integrator) and drifts at $\mu = 2.9$, and relate the drift rate to equation (22).

Problem 8 (project). The stable loop periodic orbit at $\mu = 3$, $E = 2g$ appears numerically to satisfy $|I| = E/2$. At the symmetric crossing $\theta = 0$, $p_r = 0$, equation (21) vanishes identically, so the constant must be read off elsewhere: on the other component of the fixed set of $\mathcal{R}$, at $\theta = \pi$, $p_r = 0$, equation (21) gives $|I| = 2p_\theta^2/r$. Verify numerically which component the stable loop actually crosses. Refine the orbit and compare $|I|$ with $E/2$ to as many digits as the integrator supports; the computation can fail to refute exactness, but cannot establish it. Under the scaling $r \to \lambda r$, $t \to \sqrt{\lambda}\, t$ at fixed g one has $E \to \lambda E$ and $I \to \lambda^2 I$, so the unit-free form of the conjecture is $|I| = E^2/(4g)$, which reduces to $|I| = E/2$ when $E = 2g$. For $\mu \neq 3$, where I is no longer conserved, evaluate I at the $\theta = \pi$, $p_r = 0$ crossing; does the condition $2p_\theta^2/r = E/2$ there continue to select a distinguished orbit?

Problem 9 (discussion). Describe another particle system, classical or quantum, whose description requires passing from the original configuration space to a double cover. *Hint*: consider the Levi-Civita regularization of the Kepler problem, the sign change of a spin-$\frac{1}{2}$ wavefunction under a 2π rotation, or the geometric phase acquired on a circuit around a conical intersection.

13 Conclusion

Yehia observed that SAM may be viewed as motion on a cone [24]. The contribution here is a detailed description of how the *cone angle* at the value π connects to a smooth *double cover* and, in turn, provides a more motivated derivation of the integrable case $\mu = 3$ of the swinging Atwood's machine. The geometric formulation also brings into focus why the second integral resists an elementary search in the physical variables of the original configuration space, but comes into view on the lift.

Data availability statement

The computer-algebra script used to verify equation (22) and the scripts that generate the figures are openly available at `https://doi.org/10.5281/zenodo.22084996`. No experimental data were generated in this study.

A From parabolic to physical variables

To convert equation (20) into equation (21), write $s = \sin(\theta/2)$ and $c = \cos(\theta/2)$; then $\xi^2 + \eta^2 = 4r$, $\xi^2 - \eta^2 = 4rs$ and $\xi^2\eta^2 = 4r^2c^2$, so the potential term of equation (20) is at once $4gr^2c^2s$. For the kinetic term put $u = \dot{r} = p_r/4$ and $v = \frac{1}{2}rc\,\dot{\theta} = cp_\theta/(2r)$, and set $A = u(1+s) + v$, $B = u(1-s) - v$. Differentiating $\xi^2 = 2r(1+s)$ and $\eta^2 = 2r(1-s)$ gives $\xi\dot{\xi} = A$ and $\eta\dot{\eta} = B$, so that $p_\xi = (\xi^2+\eta^2)\dot{\xi} = 4rA/\xi$ and likewise $p_\eta = 4rB/\eta$. Substituting these into the kinetic term of equation (20) and using $\eta^2/\xi^2 = (1-s)/(1+s)$, $\xi^2/\eta^2 = (1+s)/(1-s)$ and $1 - s^2 = c^2$,

$$\frac{\eta^2 p_\xi^2 - \xi^2 p_\eta^2}{2(\xi^2+\eta^2)} = 2r\,\frac{A^2(1-s)^2 - B^2(1+s)^2}{c^2}. \tag{25}$$

The bracket factors,

$$\frac{A^2(1-s)^2 - B^2(1+s)^2}{c^2} = \frac{(2v)(2uc^2 - 2vs)}{c^2} = 4uv - \frac{4v^2 s}{c^2}, \tag{26}$$

so the kinetic term is $2r(4uv - 4v^2s/c^2) = 8ruv - 8rv^2s/c^2$, whence $8ruv = p_r p_\theta c$ and $8rv^2s/c^2 = 2p_\theta^2 s/r$. Collecting the two terms gives equation (21).

References

[1] Lemos N A 2018 *Analytical Mechanics* (Cambridge: Cambridge University Press)

[2] Tufillaro N B, Abbott T A and Griffiths D J 1984 Swinging Atwood's machine *Am. J. Phys.* **52** 895–903

[3] Tufillaro N B 1986 Integrable motion of a swinging Atwood's machine *Am. J. Phys.* **54** 142–3

[4] Casasayas J, Nunes A and Tufillaro N B 1990 Swinging Atwood's machine: integrability and dynamics *J. Phys. France* **51** 1693–702

[5] Pujol O, Pérez J P, Ramis J P, Simó C, Simon S and Weil J A 2010 Swinging Atwood machine: experimental and numerical results, and a theoretical study *Physica* D **239** 1067–81

[6] Martínez R and Simó C 2011 Non-integrability of the degenerate cases of the swinging Atwood's machine using higher order variational equations *Discrete Contin. Dyn. Syst.* **29** 1–24

[7] Szumiński W and Maciejewski A J 2022 Dynamics and integrability of the swinging Atwood machine generalisations *Nonlinear Dyn.* **110** 2101–28

[8] Tufillaro N B 1994 Teardrop and heart orbits of a swinging Atwood's machine *Am. J. Phys.* **62** 231–3

[9] Nunes A, Casasayas J and Tufillaro N B 1995 Periodic orbits of the integrable swinging Atwood's machine *Am. J. Phys.* **63** 121–6

[10] Tufillaro N 2026 Tracking the spread of chaos in the swinging Atwood machine *Am. J. Phys.* **94** 688–95

[11] Whittaker E T 1937 *A Treatise on the Analytical Dynamics of Particles and Rigid Bodies* 4th edn (Cambridge: Cambridge University Press)

[12] Tufillaro N, Nunes A and Casasayas J 1988 Unbounded orbits of a swinging Atwood's machine *Am. J. Phys.* **56** 1117–20

[13] Devaney R L 1976 Reversible diffeomorphisms and flows *Trans. Am. Math. Soc.* **218** 89–113

[14] Landau L D and Lifshitz E M 1976 *Mechanics* 3rd edn (Oxford: Butterworth–Heinemann) secs 44 and 48

[15] Lanczos C 1986 *The Variational Principles of Mechanics* 4th edn (New York: Dover) ch V

[16] Gray C G and Taylor E F 2007 When action is not least *Am. J. Phys.* **75** 434–58

[17] Casetti L, Pettini M and Cohen E G D 2000 Geometric approach to Hamiltonian dynamics and statistical mechanics *Phys. Rep.* **337** 237–341

[18] Montgomery R 2023 The Kepler cone, Maclaurin duality and Jacobi–Maupertuis metrics *arXiv*:2312.08173

[19] Knauf A and Montgomery R 2023 Compactification of the energy surfaces for n bodies *Regul. Chaotic Dyn.* **28** 628–58

[20] Montgomery R 2024 *Four Open Questions for the N-Body Problem* (Cambridge: Cambridge University Press)

[21] Montgomery R 2023 Dropping bodies *Math. Intelligencer* **45** 168–74

[22] Gutzwiller M C 1973 The anisotropic Kepler problem in two dimensions *J. Math. Phys.* **14** 139–52

[23] Gutzwiller M C 1990 *Chaos in Classical and Quantum Mechanics* (New York: Springer)

[24] Yehia H M 2006 On the integrability of the motion of a heavy particle on a tilted cone and the swinging Atwood machine *Mech. Res. Commun.* **33** 711–6

[25] Thurston W P 1979 *The Geometry and Topology of Three-Manifolds* lecture notes (Princeton, NJ: Princeton University) ch 13

[26] Scott P 1983 The geometries of 3-manifolds *Bull. London Math. Soc.* **15** 401–87

[27] Levi-Civita T 1920 Sur la régularisation du problème des trois corps *Acta Math.* **42** 99–144

[28] Stiefel E L and Scheifele G 1971 *Linear and Regular Celestial Mechanics* (Berlin: Springer)

[29] Roa J 2017 *Regularization in Orbital Mechanics: Theory and Practice* (Berlin: De Gruyter)

[30] Tufillaro N B 1985 Collision orbits of a swinging Atwood's machine *J. Physique* **46** 2053–6

[31] Landau L D and Lifshitz E M 1977 *Quantum Mechanics: Non-Relativistic Theory* 3rd edn (Oxford: Pergamon) secs 37 and 77

[32] Morse P M and Feshbach H 1953 *Methods of Theoretical Physics* part I (New York: McGraw-Hill)

[33] Liouville J 1846 Sur quelques cas particuliers où les équations du mouvement d'un point matériel peuvent s'intégrer *J. Math. Pures Appl.* **11** 345–78

[34] Arnold V I 1989 *Mathematical Methods of Classical Mechanics* 2nd edn (New York: Springer) secs 45 and 49

[35] Ziglin S L 1982 Branching of solutions and nonexistence of first integrals in Hamiltonian mechanics I *Funct. Anal. Appl.* **16** 181–9

[36] Morales-Ruiz J J 1999 *Differential Galois Theory and Non-Integrability of Hamiltonian Systems* (Basel: Birkhäuser)

[37] Elmandouh A A 2016 On the integrability of the motion of 3D-swinging Atwood machine and related problems *Phys. Lett.* A **380** 989–91

[38] Herzberg G and Longuet-Higgins H C 1963 Intersection of potential energy surfaces in polyatomic molecules *Discuss. Faraday Soc.* **35** 77–82

[39] Mead C A 1992 The geometric phase in molecular systems *Rev. Mod. Phys.* **64** 51–85